https://doi.org/10.17221/80/2019-VETMED

# Evaluation of a poly(lactic-acid) scaffold filled with poly(lactide-co-glycolide)/hydroxyapatite nanofibres for reconstruction of a segmental bone defect in a canine model

*Jang Won Yun[1], Su Young Heo[3], Min Ho Lee[2], Hae Beom Lee[1]**

*[1]College of Veterinary Medicine, Chungnam National University, Dajeon, Republic of Korea*
*[2]Department of Dental Biomaterials and Institute of Biodegradable Materials, Institute of Oral Bioscience and School of Dentistry, Jeonbuk National University, Jeonju, Republic of Korea*
*[3]College of Veterinary Medicine, Jeonbuk National University Specialized Campus, Iksan, Republic of Korea*

**Corresponding author: seatiger76@cnu.ac.kr*

*Jang Won Yun and Su Young Heo contributed equally to this work*

**Citation**: Yun JW, Heo SY, Lee MH, Lee HB (2019): Evaluation of a poly(lactic-acid) scaffold filled with poly(lactide-co-glycolide)/hydroxyapatite nanofibres for reconstruction of a segmental bone defect in a canine model. Veterinarni Medicina 64, 531–538.

**Abstract**: Critical-sized bone defects are a difficult problem in both human and veterinary medicine. To address this issue, synthetic graft materials have been garnering attention. Abundant *in vitro* studies have proven the possibilities of poly(lactic-acid) (PLA) scaffolds and poly(lactide-co-glycolide)/hydroxyapatite (PLGA/HAp) nanofibres for treating bone defects. The present study aimed at conducting an *in vivo* assessment of the biological performance of a three dimensional (3D)-printed PLA scaffold filled with a PLGA/HAp nanofibrous scaffold to estimate its potential applications in bone defect reconstruction surgery. Defects were created in a 20 mm-long region of the radius bone. The defects created on the right side in six Beagle dogs ($n$ = 6) were left untreated (Group 1). The defects on the left side ($n$ = 6) were filled with 3D-printed PLA scaffolds incorporated with PLGA/HAp nanofibres with gelatine (Group 2). The other six Beagle dog defects were made bilaterally ($n$ = 12) and filled with the same material as that used in Group 2 along with recombinant bone morphogenetic protein 2 (rhBMP-2) (Group 3). Both the radiological and histological examinations were performed for observing the reaction of the scaffold and the bone. Micro-computed tomography (CT) was utilised for the evaluation of the bone parameters 20 weeks after the experiment. The radiological and histological results revealed that the scaffold was biodegradable and was replaced by new bone tissue. The micro-CT revealed that the bone parameters were significantly ($P < 0.05$) increased in Group 3. Based on these results, our study serves as a foundation for future studies on bone defect treatment using synthetic polymeric scaffolds.

**Keywords**: bone regeneration; bone tissue engineering; FDM technology; electrospinning; osteogenic factor

Treating large bone defects is a difficult problem in both human and veterinary medicine. Bone defects result from trauma, non-union, tumour resection, and revision surgery (Li et al. 2015). Various biomaterials have been tried to solve this problem. Recently, bone tissue engineer-

Supported by research funds for newly appointed professors of Jeonbuk National University in 2018.

https://doi.org/10.17221/80/2019-VETMED

ing has become a popular approach to fabricate bone substitutes. Recently, numerous *in vivo* and *in vitro* studies have demonstrated the potential applications of both poly(lactic-acid) scaffolds and poly(lactide-co-glycolide)/hydroxyapatite (PLGA/HAp) nanofibrous structures, which are fabricated using electrospinning, in bone tissue engineering (Makadia and Siegel 2011; Lipner et al. 2014; Stachewicz et al. 2015). Numerous studies have proven that poly(lactic-acid) (PLA) is suitable for three-dimensional (3D) printing with fused deposition modelling (FDM) technology to manufacture scaffolds (Gremare et al. 2018). The mechanical properties and biodegradation time can be manipulated by controlling the ratio of lactide (LA) to glycolide (GA) in PLGA, and it is, therefore, a flexible material for use in clinical applications (Lao et al. 2011). In addition to the advantages of PLGA, hydroxyapatite (HAp) is one of the most promising materials for bone tissue engineering. The nanofibres that are fabricated by electrospinning are similar to those of the natural bone extracellular matrix and may result in the additional stimulation of the cultured cells. Furthermore, cell attachment, proliferation, and mineralisation can occur because of its wide surface area (Mazaheri et al. 2015). Numerous *in vitro* studies have demonstrated the possibilities of using poly(lactic-acid) and poly(lactide-co-glycolide)/hydroxyapatite (PLGA/HAp) nanofibres for bone tissue engineering, which are fabricated using 3D printing with FDM technology and electrospinning (Lipner et al. 2014; Haider et al. 2015; Stachewicz et al. 2015; Heo et al. 2017). However, the authors of these *in vitro* reports were unable to assess the biomechanical properties of the engineered tissue. To the best of our knowledge, no *in vivo* studies have been conducted using two different types of scaffolds to mimic the real bone structure for treating segmental bone defects. The purpose of this study was to perform an *in vivo* assessment of the biological performance of gelatine and rhBMP-2-instilled 3D-printed PLA scaffolds filled with PLGA/HAp nanofibres to estimate their potential applications in segmental bone defect reconstruction in a canine model.

## MATERIAL AND METHODS

**PLGA/HAp nanofibre**. Poly(lactide-co-glycolide) (PLGA, LA/GA 70/30, MW = 200 kDa) was imported from Sigma-Aldrich Inc. (USA) for manufacturing the PLGA/HAp nanofibrous scaffold. The powder was supplied in the form of-synthetic hydroxyapatite ($Ca_3(PO_4)_2$; KT) (Fluka cat. No. 21223, Sigma-Aldrich, Gillingham, UK). The electrospun PLGA/HAp was manufactured according to the method previously described by Heo et al. (2017). Dissolution of the PLGA was performed by utilising methylene chloride (MC) and dimethylformamide (DMF) (Du Pont, Michigan, USA) at an 80/20 ratio to obtain a 10 wt% solution. HAp was added into the 10 wt% solutions to create a final mixture containing HAp of 1 wt% solids. The electrospinning was performed at a rate of 6 ml/h and applied to a 15 kV voltage by a high voltage power supply (CPS-60 K02V1, Chungpa EMT Co., Gyeonggi-do, Republic of Korea). The distance between the needle and the collector was 15 cm (Figure 1). The electrospun nanofibres were dried for one week to eliminate any remaining MC/DMF. The electrospun nanofibres were then rolled up with 5-mm pins and attached to a sheet by using MC/DMF to make the 3D electrospun nanofibrous structures. The custom-made electro-

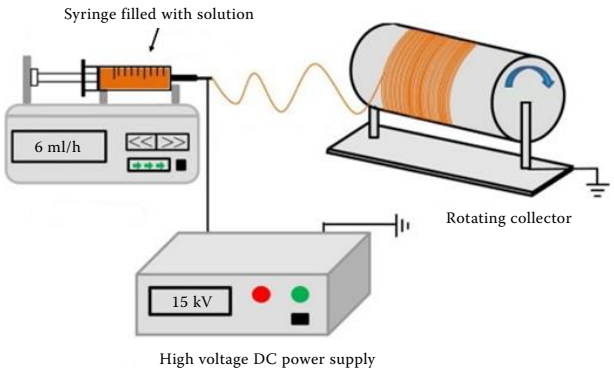


Figure 1. The electrospinning procedure

Figure 2. The schematic diagram showing the process of the three-dimensional electrospun nanofibrous scaffold

https://doi.org/10.17221/80/2019-VETMED

spun nanofibres were 5 × 10 mm$^2$ and 20 mm long, with a wall thickness of 2 mm and an oval-shaped cylindrical structure (Figure 2).

**3D-printed PLA scaffold fabrication**. All the dogs were scanned with a 32-detector row computed tomography (CT) scanner (Alexion™, Toshiba, Tokyo, Japan). After the CT images were acquired, the Digital Imaging and Communications in Medicine (DICOM) files were converted into a surface tesselation language (STL) file utilising the InVesalius 3.0 software (CTI, Campinas, Sao Paulo, Brazil) (Figure 3A). After importing the STL file for the 3D printer, Makerbot Replicator, and Replicator 2X FDM-type 3D printers (Makerbot, New York City, NY, USA), in conjunction with the Makerware software version 2.4.162, the printers were used to build a scaffold from natural a 1.77 mm PLA filament (Makerbot, New York City, NY, USA) (Figure 3B). The printing parameters were set to a standard (0.15 mm) resolution (100–200 µm) with an extruder temperature of 229 °C and an extrusion speed of 90 mm/s with a 150 mm/s traveling speed and a 0.4 mm diameter brass nozzle. The printer extruder head deposits the melted PLA layer by layer with the aid of rafts or support structures to create the intended structure (Figure 3C).

**Preparation of rhBMP-2 and gelatine**. A 1.0 mg/ml concentration of the recombinant bone morphogenetic protein 2 (rhBMP-2) solution was prepared for the experiment. The rhBMP-2 (0.25 mg; Novosis®, Daewoong CGBio, Seoul, Republic of Korea) was dissolved in 0.25 ml of distilled water. The gelatine (type B, from bovine skin, approximately 225 Bloom) was imported from Sigma-Aldrich Inc. (USA).

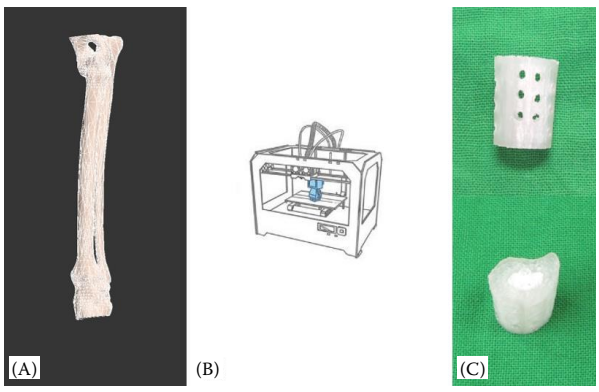


Figure 3. The surface tesselation language (STL) file (**A**). After importing the STL file for the 3D printer, the extruder head of a printer deposits the melted poly(lactic-acid) (PLA) (**B**). The PLA scaffold filled with the nanofibres scaffold (**C**)

**Experimental animals and design**. Twelve Beagle dogs (six intact males and six intact females; a mean age of 2.6 ± 0.7 years and a mean weight of 14.3 ± 2.16 kg) were used. Physical and radiographic examinations were performed to ensure the absence of any orthopaedic problem. The animals were divided into three groups. Six Beagle dogs had defects created on the right side ($n$ = 6) and were not treated (Group 1). The defects on the left side ($n$ = 6) were filled with the gelatine-instilled 3D-printed PLA scaffold filled with the PLGA/HAp nanofibre (Group 2). In the other six Beagle dogs, the defects were made bilaterally ($n$ = 12) and filled identically with the PLGA/HAp nanofibre with rh-BMP-2 (Group 3). All the animal procedures utilised in this study were duly approved by the Institutional Animal Care and Use Committee IACUC (CBNU 2015-061) of Chonbuk National University. Extra care was taken to prevent any form of pain or suffering of the animals used in the study. After the experiment was over, the Beagle dogs were euthanised using 0.5 mg/kg of intravenous T61TM (Intervet, Boxmeer, The Netherlands).

**Surgical technique**. Under general anaesthesia, a craniolateral incision was made, and each bone defect was made in a 20 mm-long region in the radius by using an oscillating saw under irrigation. Then, the scaffold was prepared for use (Figure 4A and 4B). In six Beagle dogs, the right-side defects were not treated (Group 1) (Figure 4C), and the left-side defects were filled with the scaffold and gelatine (Group 2) (Figure 4D). In the other six dogs, each defect was filled with the scaffold and gelatine along with a 1.0 mg/ml concentration of the 0.25 ml rhBMP-2 solution (Group 3)

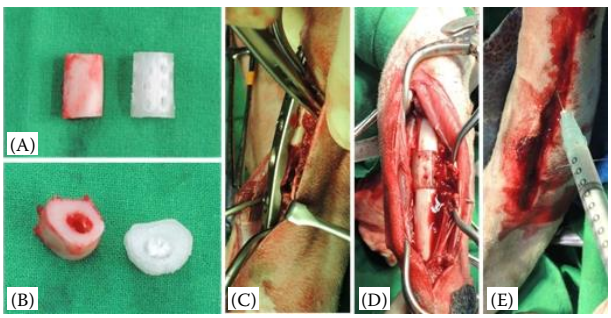


Figure 4. The resected radius bone segment (left) and the poly(lactic-acid) (PLA) scaffold filled with the PLGA/HAp nanofibre (right) (**A** and **B**). An intraoperative view of a 20 mm-long radius defect fixed with an LC-DCP plate (**C**). A scaffold inserted into defect (**D**). Implantation of the gelatine and rhBMP-2 (**E**)

https://doi.org/10.17221/80/2019-VETMED

(Figure 4E). All the defects were fixed with 7 holes using an LC-DCP (Locking Compression-Dynamic Compression Plate) and 3.5 cortical screws (Synthes, West Chester, USA). The postoperative treatment included administration of carprofen (2.2 mg/kg *p.o.*, one time daily, Rimadyl®; Pfizer Animal Health, USA) and cephalexin (15 mg/kg *p.o.*, two times daily, Methilexin Inj®, Union Korea Pharm, Republic of Korea) for 2 weeks.

**Plain radiography**. Radiographs were taken during the experimental period (postoperatively and at 2, 4, 8, 16, and 20 weeks, respectively). The radiographs were scored by three independent radiologists based on the information listed in Table 1.

**Micro-CT**. The quantitative evaluation of the defect sites was performed using an X-ray micro-CT instrument (SKYSCAN *in vivo* micro-CT SKYSCAN n.v., Kontich, Belgium). The samples were moistened by normal saline during the micro-CT scanning to prevent the sample drying. The scanning, with a resolution of 35 µm, was performed with an energy of 100 KV and intensity of 100 µA. The biopsy sections were scanned 180° at 0.4 degree intervals. We used a 0.5 mm aluminium filter to soften and even out the X-ray beams. The two-dimensional (2D) image slices were reconstructed using a cone beam volumetric algorithm (version 1.8.1.5, CT-analyzer SKYSCAN). The high and low radiopacity in mineralised tissues were differentially segmented by a two-level global thresholding procedure (Gabet et al. 2004). The 3D images were made with the software CT-Analyzer (Skyscan), and the defect sites were evaluated. The following parameters were measured in the 3D model: (I) the tissue volume (TV; $mm^3$); (II) the bone volume (BV; $mm^3$); (III) the percent bone volume (BV/TV; %); (IV) the tissue surface (TS; $mm^2$); (V) the bone surface (BS; $mm^2$); and (VI) the bone surface/volume ratio (BS/BV; 1/mm).

Table 1. The radiographic scoring system for the evaluation of the bone defect healing

| Description | scores |
|---|---|
| **Bone formation** | |
| Full gap bone formation | 4 |
| Bone formation filling 75% of the defect | 3 |
| Bone formation filling 50% of the defect | 2 |
| Bone formation filling 25% of the defect | 1 |
| No evidence of bone formation | 0 |
| **Bone union** | |
| Defect bridged by uniform new bone, cut ends of cortex not seen | 4 |
| New bone formation evident but bone defect gap not bridged | 2 |
| No evidence of healing | 0 |
| **Remodelling** | |
| Full remodelling of cortex | 4 |
| Remodelling of the intramedullary canal | 2 |
| No remodelling | 0 |
| **Sum of the radiographic scores** | 12 |

**Histological examination**. Two dogs were euthanised at four weeks, and 10 dogs were euthanised 20 weeks after surgery. The harvested biopsy was fixed in a 10% formalin solution. The defect sites were observed along the longitudinal section, and the undecalcified sections were examined. The samples were stained with Villanueva Osteochrome Bone Stain solution (Polysciences Inc., Warrington, USA) for 72 hours. Next, the samples were dehydrated in a graded series of ethanol (70, 95, and 100%) and acetone. The stained samples were embedded in poly(methyl methacrylate). The embedded blocks were cut by using a hard tissue cutting machine (Struer Accutom-50, Willich, Germany) under constant cooling by a sufficient constant rate water drop. The undecalcified sections had an initial thickness of around 100 µm and were successively ground to a thickness of approximately 50 µm using a grinding machine (Struer Rotopol-35, Willich, Germany). The histological analyses were performed to examine the newly formed bone at the scaffold using a stereoscopic microscope (Leica microsystem DE/EZ 4, Wetzlar, Germany) and an optical microscope (DM 2500 M, Leica, Wetzlar, Germany).

**Statistical analysis**. The radiographic evaluation score and micro-CT data were analysed by a one-way analysis of variance (one-way ANOVA) and Scheffe's post hoc test in SPSS (IBM SPSS, Chicago, USA). The statistical significance was set at $^*P < 0.05$. The data are expressed as the mean ± SD.

## RESULTS

### Experiment follow-up

All the experimental animals recovered well without any signs of complications. No clinical abnormalities were observed. All the animals could walk and showed normal limb weight bearing after one week.

https://doi.org/10.17221/80/2019-VETMED

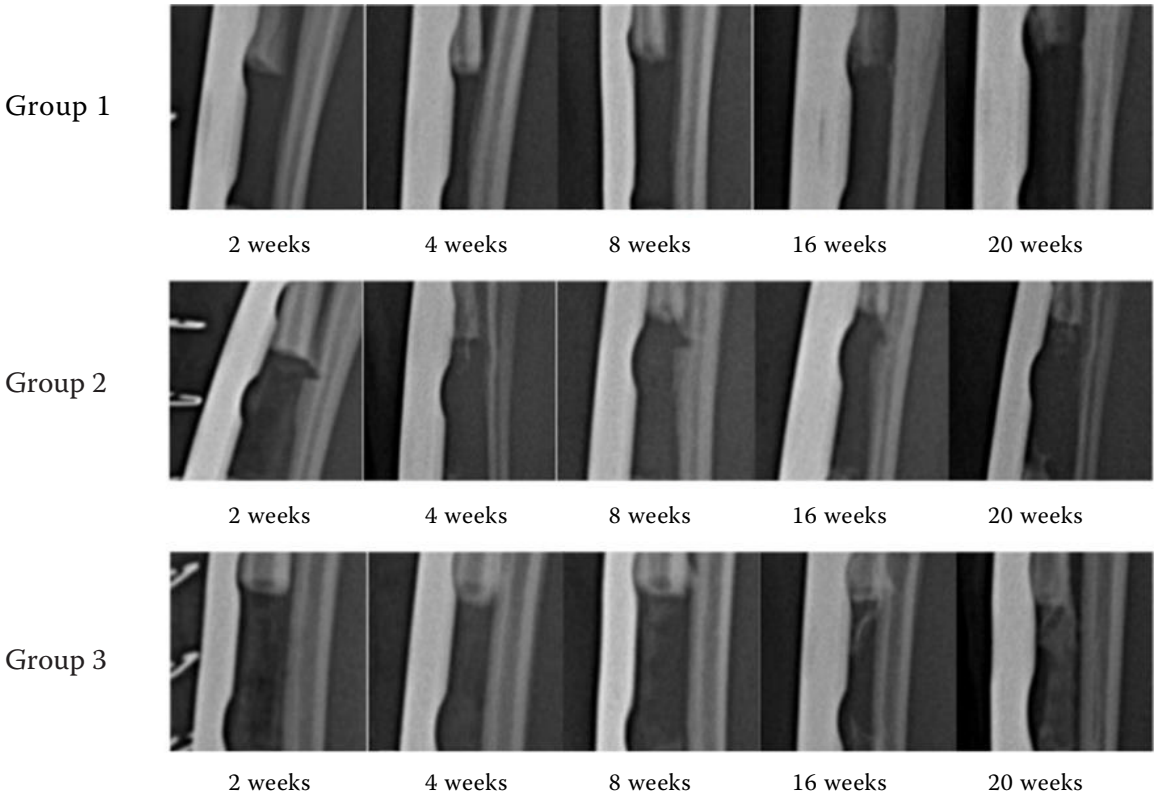


Figure 5. The representative serial radiographs of defect sites in each group at 2, 4, 8, 16, and 20 weeks post-operatively

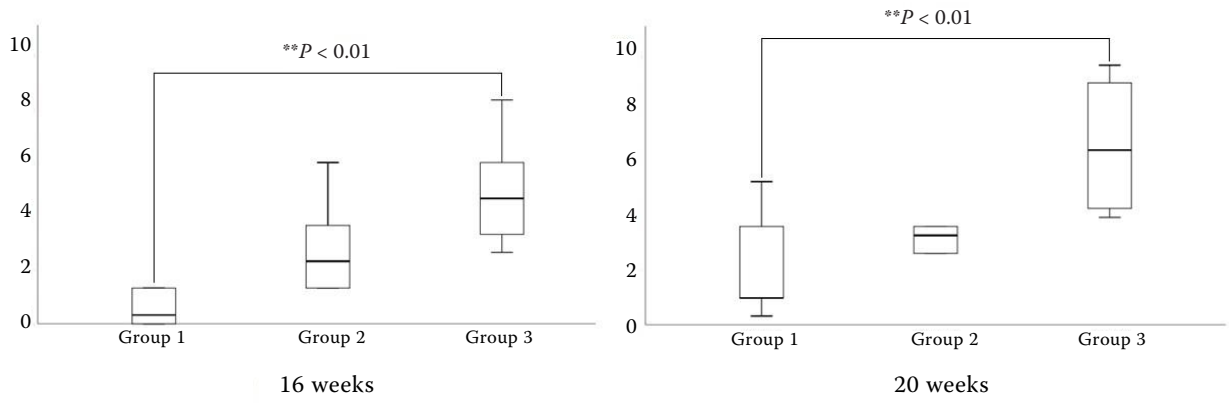


Figure 6. Significant (**$P < 0.01$) differences in the radiographic scores were observed at both 16 weeks and 20 weeks

## Plain radiography

At 16 weeks, the radiographs revealed new bone formation between the scaffold and the cutting plane of the defect in Group 3. At 20 weeks, the increased bone formation in the scaffold and bone defect connected to the defect site was seen in Group 3. In Groups 1 and 2, there was little or no bone formation in the defect at 16 and 20 weeks (Figure 5). Compared to Group 1, significant differences in the radiographic scores were observed at both 16 and 20 weeks postoperatively in Group 3 (**$P < 0.01$) (Figure 6).

## Micro-CT

The 3D reconstructed micro-CT image showed noticeable new bone formation in Group 3 compared to that in Groups 1 and 2 (Figure 7A–C). The bone

https://doi.org/10.17221/80/2019-VETMED

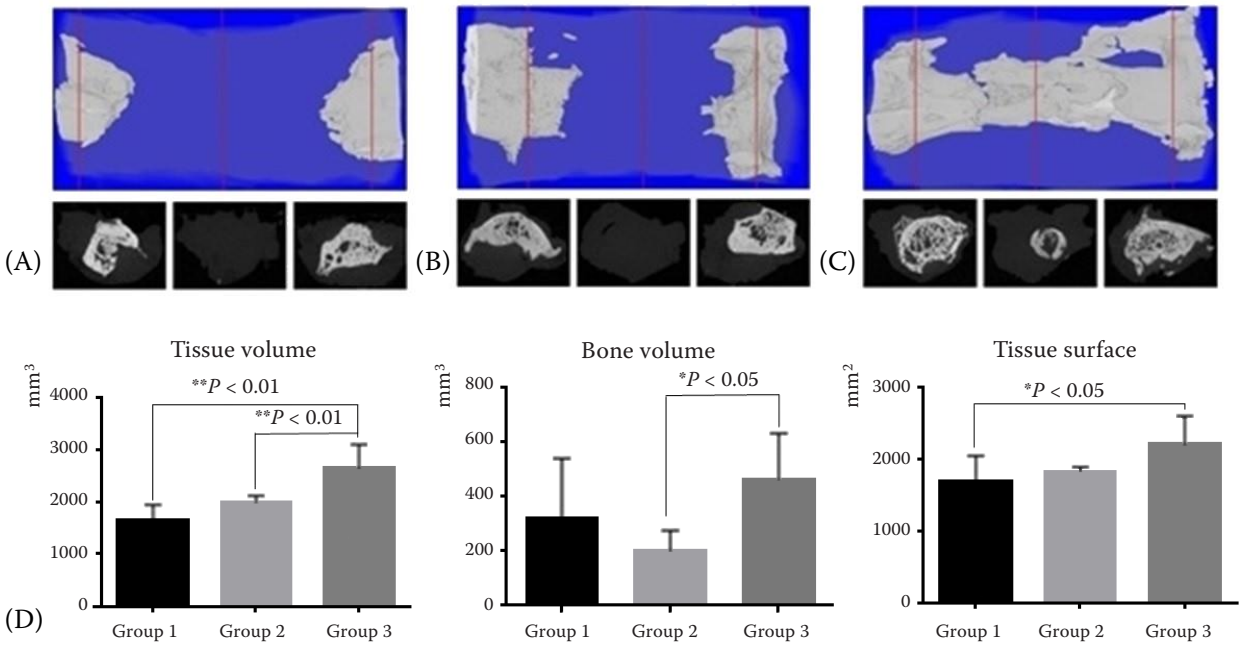


Figure 7. The representative reconstructed 3D images of the micro-CT 20 weeks after the experimentation (Group 1 (**A**), Group 2 (**B**), Group 3 (**C**)). Significant differences were observed in the bone parameters of the 3D micro-CT analysis (**D**)

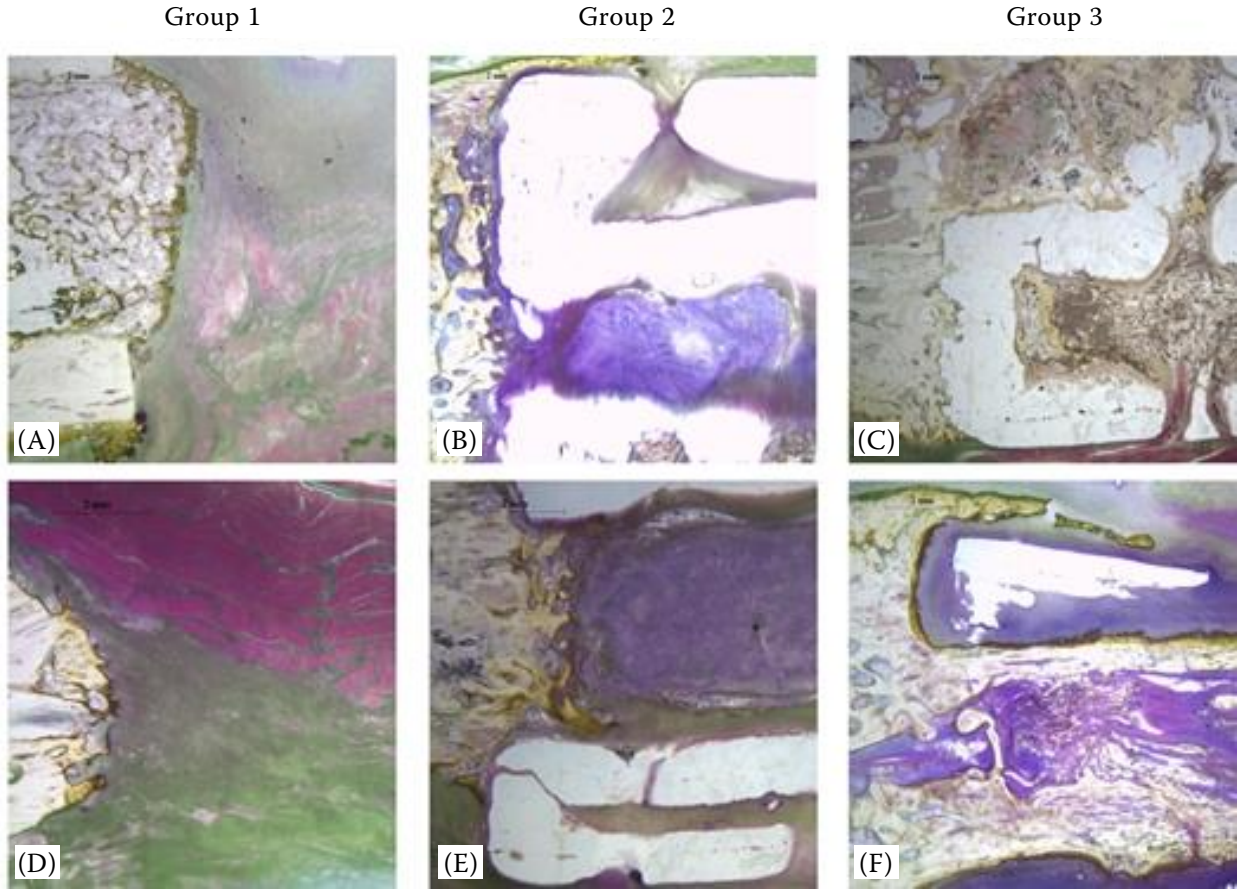


Figure 8. The photomicrograph views of the experimental site at the scaffold-host bone junction. Undecalcified sections: Original magnification × 8. Results after 4 weeks (**A**, **B**, and **C**). Results after 20 weeks (**D**, **E**, and **F**)

https://doi.org/10.17221/80/2019-VETMED

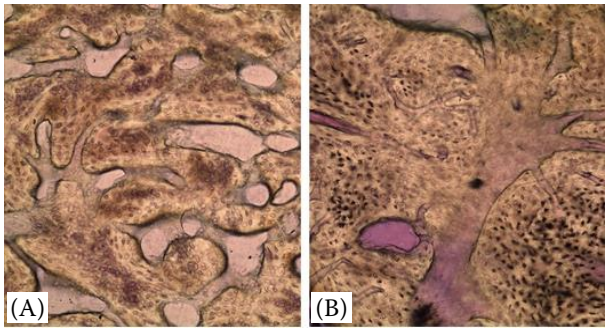


Figure 9. The photomicrograph views of the defect at 20 weeks (Group 3). Central region (**A**) and host bone-scaffold junction (**B**). The undecalcified sections: original magnification × 100

mass parameters were observed to be significantly (*$P < 0.05$) increased in Group 3. The comparative 3D micro-CT analyses are shown in Figure 7D.

### Histological examination

At 4 weeks, Group 1 showed no bone formation and only cytoplasm filled the defect (Figure 8A) whereas at the same time, Group 2 had substantial osteoblasts in the inner scaffold, as indicated by the colour purple (Figure 8B). Group 3 at 4 weeks showed considerable bony proliferation, but the PLA scaffold was barely degraded (Figure 8C). For Group 1 at 20 weeks, there were no significant differences between the results at 4 weeks (Figure 8D). For Group 2 at 20 weeks, a small amount of bony proliferation was noticed in the inner structure (Figure 8E). Group 3 at 20 weeks showed definite new bone formation activity at the PLGA/HAp nanofibre and cutting plane of the bone, and the new bone formation was fully connected to the implant via the new bone tissues (Figure 8F). Furthermore, there was considerable biodegradation in the PLA scaffold. The photomicrograph views of the implant site in Group 3 at 20 weeks showed noticeable new bone tissues. The mid-shaft region of the scaffold was still osteoporotic, and the host bone-scaffold junction was not fully bridged (Figure 9A and 9B).

## DISCUSSION AND CONCLUSIONS

All the results presented in this study demonstrate substantial new bone formation in the bone defect model in Group 3. The radiological and histological results proved that the scaffold is biodegradable and was replaced by new bone tissue. The bone parameter values for the bone and tissue volumes, and the tissue surface measured by micro-CT were observed to be significantly (*$P < 0.05$) increased in Group 3. Numerous studies have investigated bone defect treatments using polymeric scaffolds with various manufacturing methods (Murugan and Ramakrishna 2005). PLA, because of its biocompatibility, thermal stability, low viscosity, and thermoplastic properties, is well-suited for 3D-printing with FDM technology (Gremare et al. 2018). Based on this, a PLA scaffold was used as the outer structure for load sharing at the bone-scaffold junction and for biomechanical stability after the plate fixation (Talbot et al. 2008). In our study, the porosity only consisted of six 2-mm-sized holes that were made at each cranial and caudal aspect of the PLA scaffold in order to preserve the mechanical properties during the biodegradation. Gregor et al. (2017) reported that the proliferation was equally adequate for PLA scaffolds of both 30% and 50% porosity, which confirmed that it is not essential to maintain the recommended bone tissue replacement scaffold porosity at around 90%. This fact also addresses the mechanical properties issues reported for PLA scaffolds with high porosity because the scaffold allowed for the sufficient proliferation of cells and simultaneously had more material in its structure, which ensures better mechanical durability. However, the PLA scaffolds, in our study, were barely biodegraded. Adjusting the porosity and pore size can increase the degradation rate as well as enhancing the bony proliferation (Odelius et al. 2011). However, deciding the exact porosity and pore size balance of the PLA scaffold for a weight loading animal bone model which can achieve an adequate biodegradation rate and bony proliferation meanwhile achieving mechanical stability still remains unclear and further studies are needed. The PLGA/HAp nanofibrous structure was significantly replaced by bone tissue in Group 3. The nanofibrous structures mimic the natural extracellular matrix and provide a starting place for the cell attachment, proliferation, and differentiation (Bhardwaj and Kundu 2010). Our nanofibrous structures were made by using electrospinning to mimic the bone marrow and were instilled with gelatine because it is suitable for cell adhesion on the electrospun nanofibre (Heo et al. 2017). However, the bone defects transplanted with the PLGA/HAp nanofibrous scaffolds in our

https://doi.org/10.17221/80/2019-VETMED

study were not sufficiently filled with new bone tissue in Group 2. Haider et al. (2015) stated that the bulk delivery of growth factors to the site of interest through direct injection is limited and less efficient in terms of new bone generation. However, in our study, rhBMP-2 was instilled into the scaffold and induced significant bone regeneration. This study aimed at evaluating the possibility of using a gelatine and an rhBMP-2-instilled 3D-printed PLA scaffold filled with a PLGA/HAp electrospun nanofibre for the repair of segmental bone defects in a canine model. Our results showed that the scaffolds used in our study were insufficient for inducing the bone tissue regeneration on their own. However, scaffolds with rhBMP-2 as an osteogenic factor revealed a significantly enhanced bony proliferation. The comparative 3D micro-CT analysis showed significantly better values ($P < 0.05$) in the segmental bone defects treated with our scaffold with gelatine and rhBMP-2 instillation compared with the scaffold alone. Based on these results, our study provides a foundation for future studies on bone defect treatment using synthetic polymeric scaffolds.

In conclusion, our results showed that segmental bone defects in the canine long bone can be treated by the use of a gelatine and an rhBMP-2-instilled 3D-printed PLA scaffold filled with PLGA/HAp electrospun nanofibres. We observed significant bony proliferation in the scaffold used in our study. However, care should be taken when interpreting the results of our study because of the small sample size and use of only one canine breed.

## REFERENCES

Bhardwaj N, Kundu SC (2010): Electrospinning: A fascinating fiber fabrication technique. Biotechnology Advances 28, 325–347.

Gabet Y, Muller R, Regev E, Sela J, Shteyer A, Salisbury K, Chorev M, Bab I (2004): Osteogenic growth peptide modulates fracture callus structural and mechanical properties. Bone 35, 65–73.

Gregor A, Filova E, Novak M, Kronek J, Chlup H, Buzgo M, Blahnova V, Lukasova V, Bartos M, Necas A, Hosek J (2017): Designing of PLA scaffolds for bone tissue replacement fabricated by ordinary commercial 3d printer. Journal of Biological Engineering 11, 31. doi: 10.1186/s13036-017-0074-3.

Gremare A, Guduric V, Bareille R, Heroguez V, Latour S, L'heureux N, Fricain JC, Catros S, Le Nihouannen D (2018): Characterization of printed PLA scaffolds for bone tissue engineering. Journal of Biomedical Materials Research Part A 106, 887–894.

Haider A, Kim S, Huh MW, Kang IK (2015): BMP-2 grafted nHA/PLGA hybrid nanofiber scaffold stimulates osteoblastic cells growth. BioMed Research International 2015. doi: 10.1155/2015/281909.

Heo SY, Kim HY, Kim NS (2017): Evaluation of Poly(lactide-co-glycolide)/hydroxyapatite nanofibres for reconstruction of critical-sized segmental bone defects in a canine model. Veterinarni Medicina 62, 325–332.

Lao L, Wang Y, Zhu Y, Zhang Y, Gao C (2011): Poly(lactide-co-glycolide)/hydroxyapatite nanofibrous scaffolds fabricated by electrospinning for bone tissue engineering. Journal of Materials Science: Materials in Medicine 22, 1873–1884.

Li Y, Chen SK, Li L, Qin L, Wang XL, Lai YX (2015): Bone defect animal models for testing efficacy of bone substitute biomaterials. Journal of Orthopaedic Translation 3, 95–104.

Lipner J, Liu W, Liu Y, Boyle J, Genin GM, Xia Y, Thomopoulos S (2014): The mechanics of plga nanofiber scaffolds with biomimetic gradients in mineral for tendon-to-bone repair. Journal of the Mechanical Behavior Biomedical Materials 40, 59–68.

Makadia HK, Siegel SJ (2011): Poly lactic-co-glycolic acid (PLGA) as biodegradable controlled drug delivery carrier. Polymers 3, 1377–1397.

Mazaheri M, Eslahi N, Ordikhani F, Tamjid E, Simchi A (2015): Nanomedicine applications in orthopedic medicine: State of the art. International Journal of Nanomedicine 10, 6039–6053.

Murugan R, Ramakrishna S (2005): Development of nanocomposites for bone grafting. Composites Science and Technology 65, 2385–2406.

Odelius K, Hoglund A, Kumar S, Hakkarainen M, Ghosh AK, Bhatnagar N, Albertsson AC (2011): Porosity and pore size regulate the degradation product profile of polylactide. Biomacromolecules 12, 1250–1258.

Stachewicz U, Qiao T, Rawlinson SCF, Almeida FV, Li WQ, Cattell M, Barber AH (2015): 3D imaging of cell interactions with electrospun PLGA nanofiber membranes for bone regeneration. Acta Biomaterialia 27, 88–100.

Talbot M, Zdero R, Garneau D, Cole PA, Schemitsch EH (2008): Fixation of long bone segmental defects: A biomechanical study. Injury 39, 181–186.

Received: June 26, 2019
Accepted after corrections: October 29, 2019